Journal of Materials Chemistry C

PAPER

View Article Online
View Journal | View Issue

Cite this: J. Mater. Chem. C, 2014, 2, 10101

New dithienyl-diketopyrrolopyrrole-based conjugated molecules entailing electron withdrawing moieties for organic ambipolar semiconductors and photovoltaic materials†

Chenmin Yu, Zitong Liu,* Yang Yang, Jingjing Yao, Zhengxu Cai, Hewei Luo, Guanxin Zhang and Deqing Zhang*

Received 21st August 2014
Accepted 2nd October 2014

DOI: 10.1039/c4tc01872a

www.rsc.org/MaterialsC

In this paper we report two DPP-based conjugated molecules **DPPBT** and **DPPTT** in which the respective electron withdrawing moieties 2,1,3-benzothiadiazole and thiazolo[5,4-*d*]thiazole are flanked by two DPP moieties. For comparison, **DPPBZ** containing 1,4-diethynylbenzene and two DPP moieties were synthesized. HOMO/LUMO energies of **DPPBT**, **DPPTT** and **DPPBZ** were estimated on the basis of cyclic voltammetric data. Owing to the fact that LUMO energies of **DPPBT** and **DPPTT** were lowered to *ca.* −3.5 eV, thin films of both **DPPBT** and **DPPTT** exhibit ambipolar semiconducting properties under N_2 atmosphere with hole and electron mobilities up to 0.25 $cm^2\ V^{-1}\ s^{-1}$ and 0.09 $cm^2\ V^{-1}\ s^{-1}$, respectively. In comparison, thin film of **DPPBZ** just shows p-type semiconducting property. Notably, ambipolar semiconductors with relatively high carrier mobility are rarely reported for DPP-containing small conjugated molecules. Alternatively, both **DPPBT** and **DPPTT** can function as electron donors for photovoltaic materials. Thin films of **DPPTT**:$PC_{71}BM$ and **DPPBT**:$PC_{71}BM$ at a weight ratio of 1 : 1 exhibit PCEs of 4.18% and 2.44%, respectively, with V_{OC} higher than 0.95 V.

Introduction

In recent years, diketopyrrolopyrrole (DPP) and its analogues, such as dithienyl-DPP, have been widely incorporated into conjugated molecules and polymers as electron accepting moieties for organic optoelectronic materials.[1–3] This is because of its unique π-conjugated system, high optical density and exceptional stability.[4] A number of DPP-based conjugated molecules and polymers were designed and prepared for organic semiconductors with high carrier-mobilities and organic photovoltaic materials with high power conversion efficiencies.[1–5] For instance, conjugated polymer **P1** (Scheme 1) derived from dithienyl-DPP and thieno[3,2-*b*]thiophene was reported to behave as p-type semiconductor with hole mobility up to 10.5 $cm^2\ V^{-1}\ s^{-1}$.[5a] However, polymer **P2** (Scheme 1) entailing dithienyl-DPP and selenophene moieties in the conjugated backbone behaved as an ambipolar semiconductor with hole and electron mobilities higher than 4.0 $cm^2\ V^{-1}\ s^{-1}$.[5b] Low band-gap conjugated polymers **P3** and **P4** (Scheme 1) were successfully utilized as electron donors for organic photovoltaic cells (OPVs) with power conversion efficiencies (PCEs) above 7.0%.[5c] However, conjugated polymers have batch-to-batch variation in terms of molecular weight and polydispersity that will affect the processability, microstructure, and thus semiconducting performances.[6–11]

In comparison, conjugated molecules are advantageous over conjugated polymers; they can be more easily functionalized and purified, thus device reproducibility can be improved. In addition, small conjugated molecules tend to self-assemble into ordered domains and their intermolecular arrangements can be

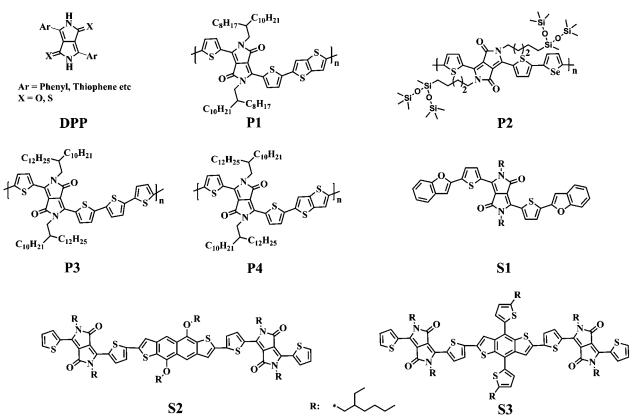

Scheme 1 Chemical structures of representative DPP-containing conjugated polymers and small molecules.

Beijing National Laboratory for Molecular Sciences, Organic Solids Laboratory, Institute of Chemistry, Chinese Academy of Sciences, Beijing 100190, China. E-mail: dqzhang@iccas.ac.cn

† Electronic supplementary information (ESI) available. See DOI: 10.1039/c4tc01872a

clarified by crystal structural analysis.[12–19] Consequently, structure–property correlations can be investigated. Therefore, small conjugated molecules have attracted increasing interests in recent years.[20,21] Scheme 1 shows several small conjugated molecules **S1**, **S2** and **S3** derived from dithienyl-DPP.[21] They all were investigated as electron donors to fabricate OPVs after blending with either [6,6]-phenyl-C_{71}-butyric acid methyl ester ($PC_{71}BM$) or [6,6]-phenyl-C_{61}-butyric acid methyl ester ($PC_{61}BM$). For instance, PCE up to 5.79% was reported for the blending thin film of **S3** with $PC_{71}BM$ as the active layer of the solar cell.[21c] Moreover, the semiconducting properties of their thin films were examined by the fabrication of the field effect transistors; they all behaved as p-type semiconductors with rather low hole mobilities.

It is known that ambipolar semiconductors are highly demanding for the fabrication of organic circuits.[22] However, ambipolar semiconductors with carrier mobilities higher than 0.1 $cm^2\ V^{-1}\ s^{-1}$ were seldom reported for DPP-based small conjugated molecules.[23] This is probably because of the fact that the lowest unoccupied molecular orbital (LUMO) energy level of DPP is relatively high; for instance, the LUMO energy level of dithienyl-DPP was estimated to be −3.29 eV. The efficient approach to lower the LUMO energy is to incorporate additional electron withdrawing moieties into the DPP-based conjugated molecules. In this paper, we report two DPP-based conjugated molecules **DPPBT** and **DPPTT** (Scheme 2) entailing additional electron accepting moieties, 2,1,3-benzothiadiazole (**BT**)[5e] and thiazolo[5,4-*d*]thiazole (**TT**),[20b–d] respectively. Both **BT** and **TT** are flanked by two DPP moieties and connected by acetylene bonds. For comparison, **DPPBZ** containing 1,4-diethynylbenzene and two DPP moieties were synthesized. The results reveal that LUMO energies of **DPPBT** and **DPPTT** are lowered to *ca.* −3.50 eV, and they both exhibit ambipolar semiconducting behaviour with hole and electron mobilities up to 0.25 $cm^2\ V^{-1}\ s^{-1}$ and 0.09 $cm^2\ V^{-1}\ s^{-1}$ for **DPPTT**, 0.045 $cm^2\ V^{-1}\ s^{-1}$ and 0.01 $cm^2\ V^{-1}\ s^{-1}$ for **DPPBT**. In comparison, a thin film of **DPPBZ** just shows p-type semiconducting property. Furthermore, both **DPPBT** and **DPPTT** show strong absorptions in the visible region and they can be utilized as photovoltaic materials as electron donors. The power conversion efficiency (PCE) of the blending thin film of **DPPTT**:$PC_{71}BM$ reaches 4.18% under standard condition.

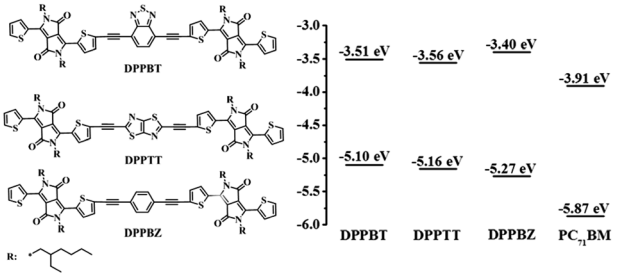

Scheme 2 Molecular structures of DPPBT, DPPTT, DPPBZ and their LUMO/HOMO energy levels, as well as those of $PC_{71}BM$.

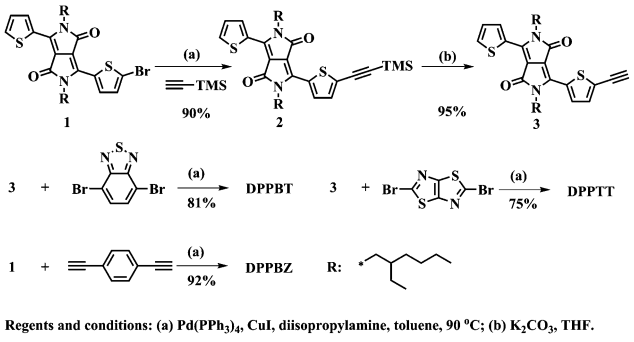

Scheme 3 Synthetic routes to DPPBT and DPPTT, as well as DPPBZ.

Results and discussion

Synthesis and characterization

The synthesis of **DPPBT**, **DPPTT** and **DPPBZ** is shown in Scheme 3. The Sonogashira coupling of **1**, which was synthesized according to the reported procedures,[21b] with ethynyltrimethylsilane afforded compound **2** in 90% yield. The removal of TMS group in **2** led to **3**, which was allowed to react with 4,7-dibromobenzo[*c*][1,2,5]thiadiazole and 2,5-dibromothiazolo-[5,4-*d*]thiazole to obtain **DPPBT** and **DPPTT** in 81% and 75% yields, respectively. Chemical structures of **DPPBT** and **DPPTT** were characterized with NMR and MS data and their purities were confirmed with elemental analysis. For comparison, **DPPBZ** (Scheme 3) in which two DPP moieties are connected by 1,4-diethynylbenzene was synthesized and fully characterized. On the basis of the thermogravimetric analysis (TGA) data shown in Fig. S1,† the thermal decomposition (at 5% weight loss) temperatures of **DPPBT** and **DPPTT** were higher than 350 °C. On the basis of the differential scanning calorimetry (DSC) data (see Fig. S1†), broad phase transitions around 215 °C were observed for **DPPTT** and **DPPBZ**, whereas **DPPBT** displayed relatively sharp transition around 220 °C. Thus, it may be concluded that solid samples of **DPPTT** and **DPPBZ** show low crystallinity.

HOMO/LUMO energies

The cyclic voltammograms of **DPPBT** and **DPPTT**, as well as **DPPBZ** were measured as shown in Fig. 1. Both **DPPBT** and **DPPTT** displayed two quasi-reversible oxidation waves and two reversible reduction waves. Compared to **DPPBZ**, the reduction waves of **DPPBT** and **DPPTT** were slightly positively shifted (see Fig. 1). This is obviously due to the respective electron withdrawing effects of **BT** and **TT** in **DPPBT** and **DPPTT**. Based on their onset oxidation and reduction potentials, the highest occupied molecular orbital (HOMO) and the lowest unoccupied molecular orbital (LUMO) energies of **DPPBT**, **DPPTT** and **DPPBZ** were estimated by the following equations and listed in Table 1: LUMO $= -(E_{red1}^{onset} + 4.41)$ eV, HOMO $= -(E_{ox1}^{onset} + 4.41)$ eV. The LUMO levels of **DPPBT** and **DPPTT** were lowered and HOMO levels were enhanced in comparison with those of **DPPBZ**. Moreover, **DPPBT** and **DPPTT** exhibited narrower bandgaps (~1.6 eV) than **DPPBZ**. HOMO/LUMO levels of **DPPBT**

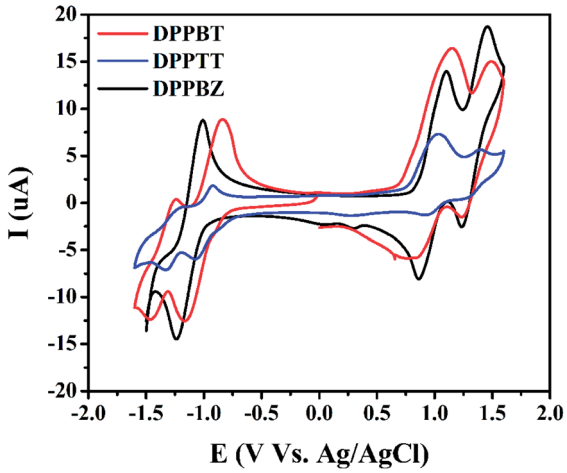

Fig. 1 Cyclic voltammograms of **DPPBT**, **DPPTT** and **DPPBZ** (1.0×10^{-3} M) in CH_2Cl_2 at a scan rate of 50 mV s^{-1}, with Pt as the working and counter electrodes and an Ag/AgCl electrode (saturated KCl) as the reference electrode, and n-Bu_4NPF_6 (0.1 M) as supporting electrolyte.

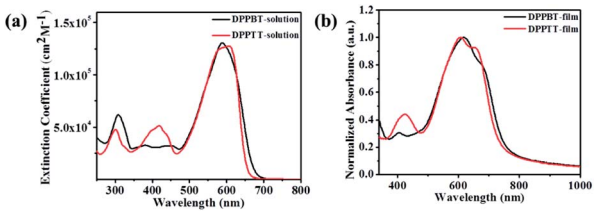

Fig. 2 UV-vis absorption spectra of **DPPBT** and **DPPTT** in $CHCl_3$ (1.0×10^{-5} M) solutions (a) and their thin films (b).

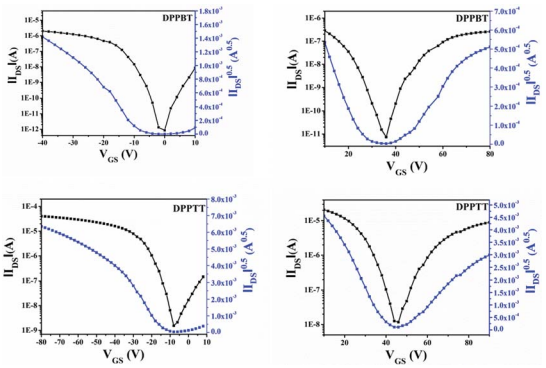

Fig. 3 Transfer characteristics (measured under N_2 atmosphere) of OFETs based on **DPPBT** and **DPPTT** after thermal annealing at 100 °C.

and **DPPTT** may enable them to behave as ambipolar semiconductors according to previous reports.[24]

Fig. 2 and S2† show the absorption spectra of the solutions and thin films of **DPPBT**, **DPPTT** and **DPPBZ**. **DPPBT** in solution strongly absorbed around 590 nm (ε_{max} = 130 000 cm^2 M^{-1}) with broad full width of 120 nm at a half maximum, whereas **DPPTT** in solution showed three absorptions around 420 (ε_{max} = 51 000 cm^2 M^{-1}), 580 (ε_{max} = 122 000 cm^2 M^{-1}) and 610 nm (ε_{max} = 127 000 cm^2 M^{-1}). In comparison, the absorption spectra of thin films of **DPPBT** and **DPPTT** were red-shifted as displayed in Fig. 2; they show strong absorptions around 620 nm and the absorption tails were extended to *ca.* 850 nm. This may be due to the intermolecular π–π interactions. The respective optical bandgaps of **DPPBT** and **DPPTT** were estimated to be 1.60 eV and 1.62 eV on the basis of their onset absorptions. The optical band gaps were in good agreement with those determined with cyclic voltammetric data (see Table 1).

The fact that both **DPPBT** and **DPPTT** show strong absorptions in the visible region with high molar absorption coefficients and narrow bandgaps may allow them to be used as photovoltaic materials. Scheme 2 demonstrates the HOMO/LUMO levels of **DPPBT** and **DPPTT** and those of $PC_{71}BM$. Judging from the energy levels, both **DPPBT** and **DPPTT** are suitable as electron donors in organic photovoltaic cells (OPVs). Moreover, the energy differences between the HOMO levels of **DPPBT** and **DPPTT** and the LUMO level of $PC_{71}BM$ were higher than 1.2 eV, thus high open-circuit voltages (V_{OC}) are expected for OPVs with **DPPBT** and **DPPTT** as donors after combining with $PC_{71}BM$ as the acceptor.

Ambipolar semiconducting properties

In order to investigate the semiconducting behaviors of **DPPBT** and **DPPTT**, as well as **DPPBZ**, the respective bottom-gate/bottom-contact organic field effect transistors (OFETs) were fabricated with conventional techniques (see Experimental section). On the basis of the respective transfer and output characteristics shown in Fig. 3 and S3,† it can be concluded that

Table 1 Absorption and electrochemical data, HOMO/LUMO energies and bandgaps of **DPPBT** and **DPPTT**, as well as **DPPBZ**

Compd.	λ_{max}/solution[a] (nm)	λ_{max}/film (nm)	E_{ox1}^{onset}[c] (V)	E_{red1}^{onset}[c] (V)	LUMO (eV) exp[d]	HOMO (eV) exp[d]	E_g (eV)
DPPBT	590(130 000)[b]	678, 618, 404	0.69	−0.90	−3.51	−5.10	1.59[e] (1.60)[f]
DPPTT	610(127 000)[b] 580(122 000)[b] 420(51 000)[b]	654, 608, 424	0.75	−0.84	−3.56	−5.16	1.60[e] (1.62)[f]
DPPBZ	592(111 000)[b] 558(95 000)[b], 386(44 000)[b]	618, 574, 398	0.86	−1.01	−3.40	−5.27	1.87[e] (1.78)[f]

[a] Measured in $CHCl_3$ solutions (1.0×10^{-5} M). [b] Molar extinction coefficient (ε_{max}). [c] In CH_2Cl_2 solutions containing Bu_4NPF_6 (0.1 M) at a scan rate of 50 mV s^{-1}. [d] Estimated from the following equations: LUMO = $-(E_{red1}^{onset} + 4.41)$ eV, HOMO = $-(E_{ox1}^{onset} + 4.41)$ eV. [e] Based on redox potentials. [f] Based on the onset absorptions of the thin films.

Table 2 OFET performance data for thin films of DPPBT and DPPTT, as well as DPPBZ

Compd.	T (°C)	μ_h[a] ($cm^2\ V^{-1}\ s^{-1}$)	$I_{on/off}$	V_{th} (V)	μ_e[a] ($cm^2\ V^{-1}\ s^{-1}$)	$I_{on/off}$	V_{th} (V)
DPPBT	Rt	3×10^{-3} (5×10^{-3})	10^4–10^5	−10–0	2.1×10^{-4} (4.0×10^{-4})	10–30	40–60
	100	0.028 (0.045)	10^4–10^5	−15–8	8×10^{-3} (1×10^{-2})	10–50	40–64
	120	0.019 (0.024)	10^4–10^5	−15–5	3×10^{-3} (5×10^{-3})	10–50	50–60
DPPTT	Rt	0.07 (0.09)	10^4–10^5	−8–3	5.0×10^{-4} (1.2×10^{-3})	10–20	40–70
	100	0.17 (0.25)	10^4–10^5	−15–6	6.5×10^{-2} (9.0×10^{-2})	10–40	45–65
	120	0.11 (0.18)	10^4–10^5	−15–5	1.4×10^{-2} (2.4×10^{-2})	10–40	40–55
DPPBZ	Rt	0.01 (0.02)	10^5	−5–10			
	100	0.11 (0.18)	10^5	−12–5			
	120	0.03 (0.05)	10^5	−12–4			

[a] The mobilities were provided in "average (highest)" form, and the performance data were obtained based on more than 20 different devices.

the thin films of **DPPBT** and **DPPTT** show ambipolar semiconducting properties under N_2 atmosphere, whereas thin film of **DPPBZ** behaves as p-type semiconductor (Fig. S4†). This agrees well with the HOMO/LUMO energies of **DPPBT** and **DPPTT**, as well as **DPPBZ**. The LUMO energies of **DPPBT** and **DPPTT** need to be further lowered in order to yield air-stable ambipolar semiconductors.

The performance data of OFETs based on thin films of **DPPBT** and **DPPTT**, as well as **DPPBZ** before and after thermal annealing are summarized in Table 2. The μ_h and μ_e of the as-prepared OFET with thin film of **DPPTT** were measured to be 0.09 $cm^2\ V^{-1}\ s^{-1}$ and 0.0012 $cm^2\ V^{-1}\ s^{-1}$, respectively. Notably, both μ_h and μ_e increased to 0.25 $cm^2\ V^{-1}\ s^{-1}$ and 0.090 $cm^2\ V^{-1}\ s^{-1}$, respectively, after annealing at 100 °C for 1.0 h. However, μ_h and μ_e started to decrease after further annealing at higher temperature. Similar trend was observed for thin film of **DPPBT**, and μ_h and μ_e reached 0.045 $cm^2\ V^{-1}\ s^{-1}$ and 0.01 $cm^2\ V^{-1}\ s^{-1}$, respectively, after thermal annealing at 100 °C for 1 h. The $I_{on/off}$ is relatively high for the hole conducting channel, whereas it is low for the electron conducting channel. It should be noted that DPP-based small conjugated molecules exhibiting ambipolar semiconducting behaviors with relatively balanced μ_h/μ_e are rarely reported. In comparison, **DPPBZ** was found to show only p-type semiconducting properties under the same condition. The hole mobility for thin film of **DPPBZ** increased to 0.18 $cm^2\ V^{-1}\ s^{-1}$ after annealing at 100 °C for 1 h (see Table 2).

Thin films of **DPPBT** and **DPPTT**, as well as **DPPBZ** before and after thermal annealing were characterized with grazing incidence X-ray diffraction (GIXRD) and atomic force microscope (AFM). As depicted in Fig. S5,† no sharp diffraction peaks were detected for their thin films even after thermal annealing in both in-plane and out-of-plane modes. Thus, their thin films show poor crystallinity. In the out-of-plane mode, broad and weak diffraction signals around 20° were detected for the thin films of **DPPBT** and **DPPTT**, as well as **DPPBZ**. This may be because of the weak intermolecular π–π interactions within the thin films. In particular, the intensity of the diffraction signal around 7° was slightly enhanced for thin film of **DPPTT** after thermal annealing at 100 °C. This may partially explain the observation that both hole and electron mobilities increase after thermal annealing.

Fig. 4 shows the AFM images of thin-films of **DPPBT** and **DPPTT** on *n*-octadecyltrichlorosilane (OTS)-modified SiO_2 substrates before and after annealing at 100 °C. Heights and sizes of molecular domains within thin films of **DPPBT** and **DPPTT** were not significantly altered after thermal annealing. The root-mean-square roughness (R_{RMS}) was changed from 0.324 nm to 0.433 nm for **DPPBT** and 0.525 nm to 0.635 nm for **DPPTT**. This may be due to the partial crystallization of molecules of **DPPBT** and **DPPTT** within their thin films after thermal annealing. For thin film of **DPPBZ**, obvious morphological variation occurred and large molecular domains were formed after thermal annealing (see Fig. S6†).

Electron donors for photovoltaic materials

Judging from their LUMO/HOMO levels (see Scheme 2), **DPPBT** and **DPPTT** may function as electron donors for photovoltaic materials as discussed above. In fact, the blending thin films **DPPBT**:$PC_{71}PM$ and **DPPTT**:$PC_{71}PM$ exhibited broad absorptions in the region of 340–760 nm with absorption maxima at 620 nm and 600 nm, respectively, as shown in Fig. S7.† Blending thin films of **DPPBT**/**DPPTT** with $PC_{71}BM$ in different weight ratios were employed as active layers for the fabrication of OPVs

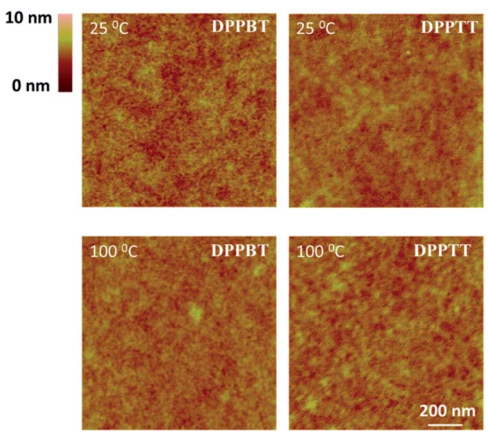

Fig. 4 AFM height images (2.0 μm × 2.0 μm) of the as-prepared thin films of DPPBT and DPPTT and those after thermal annealing at 100 °C.

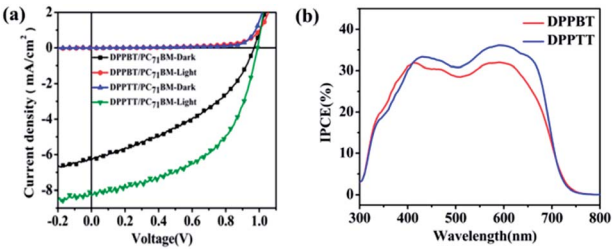

Fig. 5 (a) *I*–*V* curves of OPVs with the respective blending thin films of DPPBT/DPPTT and $PC_{71}BM$ (1 : 1); (b) IPCE spectra of OPVs with the respective blending thin films of DPPBT/DPPTT and $PC_{71}BM$ (1 : 1).

Table 3 Optimized photovoltaic performances with DPPBT and DPPTT after blending with $PC_{71}BM$[a]

Donor–acceptor	Ratio (w/w)	V_{OC} (V)	J_{SC} (mA cm^{-2})	FF (%)	PCE (%)
DPPBT:$PC_{71}BM$	1 : 1[b]	0.97	6.29	40.0	2.11 (2.44)[c]
DPPTT:$PC_{71}BM$	1 : 1[b]	0.99	8.28	51.0	3.92 (4.18)[c]

[a] The data were based on more than 10 devices. [b] With as casted thin film. [c] Data were provided in "average (highest)" form.

with the configuration of indium tin oxide (ITO)/poly(3,4-ethylenedioxythiophene):poly(styrene sulfonate) (PEDOT:PSS)/active layer/Ca/Al. The respective photovoltaic performance data based on the curves shown in Fig. 5 are summarized in Table 3. The blending thin films of both **DPPBT**:$PC_{71}BM$ and **DPPTT**:$PC_{71}BM$ exhibited best photovoltaic performance at 1 : 1 weight ratio. The **DPPBT**:$PC_{71}BM$ thin film led to a maximum PCE of 2.44%, whereas the PCE for the **DPPTT**:$PC_{71}BM$ thin film could reach 4.18%. These OPVs displayed relatively high open-circuit voltage (V_{OC}) up to 0.99 V, but the respective short-circuit current density (J_{SC}) and fill factor (FF) were not high (see Table 3). These can be enhanced by improving the order of degree of intermolecular arrangements and electron donor–acceptor interfacial structures. Thermal annealing or introduction of additives could not obviously improve the photovoltaic performances for the blending thin films of **DPPBT** and **DPPTT** with $PC_{71}BM$ under current device configuration.

As depicted in Fig. 5, the blending thin films of both **DPPBT**:$PC_{71}BM$ (1 : 1, w/w) and **DPPTT**:$PC_{71}BM$ (1 : 1, w/w) display broad IPCE (incident photon to converted current efficiency) spectra from 300 to 750 nm. These IPCE spectra correspond well to the respective UV/vis absorption profiles (Fig. S2 and S7†). The monochromatic IPCEs reach 32% at 593 nm for **DPPBT**:$PC_{71}BM$ (1 : 1, w/w) and 37% at 595 nm for **DPPTT**:$PC_{71}BM$ (1 : 1, w/w).

The blending thin films of **DPPBT**:$PC_{71}BM$ (1 : 1, w/w) and **DPPTT**:$PC_{71}BM$ (1 : 1, w/w) were characterized with GIXRD and AFM. No sharp diffraction signals were detected for both the blending thin films in both in-plane and out-of-plane modes (see Fig. S8†), indicating the order degree of intermolecular arrangements is low for both the blending thin films. Broad weak diffraction peaks from 16° to 28° and from 13° to 22° were detected for the **DPPBT**:$PC_{71}BM$ (1 : 1, w/w) thin film in the respective out-of-plane and in-plane modes. Similar broad diffraction peaks were observed for the blending thin film of **DPPTT**:$PC_{71}BM$ (1 : 1, w/w). These weak diffraction peaks may implicate the existence of intermolecular π–π interactions within the thin films, which are beneficial for improving the photovoltaic performances.

Fig. 6 shows AFM height and phase images of the blending films of **DPPBT**/**DPPTT** with $PC_{71}BM$ (1 : 1, w/w) without any post-treatments. The blending film of **DPPBT**:$PC_{71}BM$ exhibits crystalline domains and smooth surface with a root-mean-square (RMS) roughness of 0.437 nm. Moreover, the phase contrast was not obvious from the respective phase image. However, For **DPPTT**:$PC_{71}BM$ blending thin film, spherical crystalline domains with sizes of ~1700 nm^2 were detected and RMS roughness was measured to be 0.966 nm. The phase image indicates the separation of donor and acceptor domains. Therefore, these AFM images were in good agreement with the observation that the blending thin film of **DPPTT**:$PC_{71}BM$ shows better photovoltaic performance than that of **DPPBT**:$PC_{71}BM$ (see Table 3).

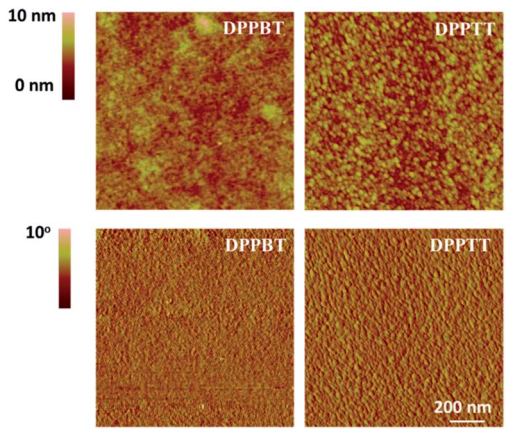

Fig. 6 AFM height and phase images (2.0 μm × 2.0 μm) of as-prepared thin films of DPPBT and DPPTT with $PC_{71}BM$ (1 : 1, w/w).

Conclusions

Two DPP-based conjugated molecules **DPPBT** and **DPPTT** were designed and synthesized. **DPPBT** and **DPPTT** entail the electron withdrawing moieties 2,1,3-benzothiadiazole (**BT**) and thiazolo[5,4-*d*]thiazole (**TT**), respectively, and the conjugated moieties are connected with acetylene bonds. The LUMO energies of **DPPBT** and **DPPTT** were lowered to −3.51 eV and −3.56 eV, respectively, on the basis of the cyclic voltammetric data. Both **DPPBT** and **DPPTT** strongly absorb in the visible region with relatively narrow optical gaps. The thin films of both **DPPBT** and **DPPTT** exhibited ambipolar semiconducting properties under N_2 atmosphere with hole and electron mobilities up to 0.045 cm^2 V^{-1} s^{-1} and 0.01 cm^2 V^{-1} s^{-1} for **DPPBT**, and 0.25 cm^2 V^{-1} s^{-1} and 0.09 cm^2 V^{-1} s^{-1} for **DPPTT** based on the characterization of the respective OFETs. In comparison, a thin film of **DPPBZ**, which contains no electron accepting moiety just shows p-type semiconducting property. In addition, **DPPBT** and

DPPTT can function as electron donors for photovoltaic materials in paring with $PC_{71}BM$ based on the consideration of their HOMO/LUMO energies and strong absorptions in the visible region. The thin films of **DPPTT**:$PC_{71}BM$ and **DPPBT**:$PC_{71}BM$ in a weight ratio of 1 : 1 exhibit a PCEs of 4.18% and 2.44% with V_{OC} higher than 0.95 V, respectively. X-ray diffraction and AFM studies reveal that the thin films of **DPPTT**:$PC_{71}BM$ and **DPPBT**:$PC_{71}BM$ show low order degree of intermolecular arrangements, and further studies to tune the intermolecular arrangements and thin film morphologies are under way.

Experimental section

Materials and characterization techniques

The reagents and starting materials employed were commercially available and used without any further purification if not specified elsewhere. Compound **1** was synthesized according to reported procedures.[21b] ^{1}H-NMR and ^{13}C-NMR spectra were recorded on Bruker AVANCE III 400/300 MHz spectrometer. Elemental analysis was performed on a Carlo Erba model 1160 elemental analyzer. MALDI-TOF MS were recorded with BEFLEX III spectrometer. TGA and DSC measurements were carried out on a SHIMADZU DTG-60 instrument under a dry nitrogen flow, heating from room temperature to 550 °C, with a heating rate of 10 °C min^{-1}. Absorption spectra were measured with JASCO V-570 UV-vis spectrophotometer. Cyclic voltammetric measurements were carried out in a conventional three-electrode cell using Pt wires of 2.0 mm diameter as working and counter electrodes, and Ag/AgCl as reference electrode on a computer-controlled CHI660C instruments at room temperature. The GIXRD data were measured at 1W1A, Beijing Synchrotron Radiation Facility. Atomic force microscopy (AFM) images of the thin films were obtained on a Nanoscope IIIa AFM (digital instruments) operating in tapping mode.

Synthesis of compound 2

Compound **1** (600 mg, 1.0 mmol), $Pd(PPh_3)_4$ (23.1 mg, 0.02 mmol), and CuI (1.1 mg, 0.006 mmol) were loaded into a flame-dried one-neck flask mounted with a condenser. Degassed/anhydrous toluene (20 mL) and $(i\text{-}Pr)_2NH$ (5 mL) were added, followed by the addition of ethynyltrimethylsilane (196 mg, 2 mmol). Then, the reaction mixture was heated to 90 °C and stirred overnight. After cooling to room temperature, 25 mL of water was added and the mixture was extracted three times with 25 mL of ethyl acetate. The organic phase was dried over Na_2SO_4 and filtered. Then, the filtrate was concentrated under reduced pressure to afford compound **2** (557 mg) in 90% yield. The crude product was used for the next step without further purification.

Synthesis of compound 3

K_2CO_3 (138 mg, 1 mmol) was added to a stirred solution of compound **2** (500 mg, 0.8 mmol) in CH_2Cl_2 (40 mL) at 25 °C, and the reaction mixture was stirred for 30 min. 10 mL of water was added and the mixture was extracted three times with 50 mL of ethyl acetate. The organic phase was dried over Na_2SO_4 and filtered. Then, the filtrate was concentrated under reduced pressure. The crude product was purified *via* flash chromatography with CH_2Cl_2/*n*-hexane (v/v, 1 : 3) as eluent to afford compound **3** (417 mg) in 95% yield. Mp 160.1–161.9 °C. ^{1}H NMR (400 MHz, $CDCl_3$, ppm): $\delta = 8.93$ (d, $J = 4$ Hz, 1H), 8.80 (d, $J = 4$ Hz, 1H), 7.65 (d, $J = 4$ Hz, 1H), 7.38 (d, $J = 4$ Hz, 1H), 7.29 (d, $J = 4$ Hz, 1H), 4.04–3.97 (m, 4H), 3.58 (s, 1H), 1.86 (br, 2H), 1.38–1.32 (m, 16H), 0.90–0.86 (m, 12H); ^{13}C NMR (75 MHz, $CDCl_3$, ppm): $\delta = 161.7$, 161.5, 141.1, 139.0, 135.8, 134.7, 134.0, 131.0, 130.9, 129.9, 129.7, 128.5, 126.6, 109.0, 108.0, 85.2, 46.0, 45.9, 39.2, 39.1, 31.9, 30.2, 29.7, 29.3, 28.3, 28.3, 27.2, 25.5, 23.5, 23.1, 22.7, 14.1, 14.0, 10.5; MS (MALDI-TOF): *m*/*z* calcd for $C_{32}H_{41}N_2O_2S_2$ $(M + H)^+$ 548.8, found 548.4; anal. calcd for $C_{32}H_{40}N_2O_2S_2$: C, 70.03; H, 7.35; N, 5.10; S, 11.69; found: C, 70.07; H, 7.37; N, 5.05; S, 11.64%.

Synthesis of DPPBT

Compound **3** (550 mg, 1 mmol), $Pd(PPh_3)_4$ (23.1 mg, 0.02 mmol), and CuI (1.1 mg, 0.006 mmol) were loaded into a flame-dried one-neck flask mounted with a condenser. Degassed/anhydrous toluene (20 mL) and $(i\text{-}Pr)_2NH$ (5 mL) were added, followed by the addition of 4,7-dibromobenzo[*c*][1,2,5]thiadiazole (117 mg, 0.4 mmol). Then, the reaction mixture was heated to 90 °C and stirred overnight. After cooling to room temperature, 25 mL of water was added and the mixture was extracted three times with 25 mL of ethyl acetate. The organic phase was dried over Na_2SO_4 and filtered. Then, the filtrate was concentrated under reduced pressure. The crude product was purified *via* flash chromatography with CH_2Cl_2/*n*-hexane (v/v, 1 : 2) as eluent to afford **DPPBT** (397 mg) in 81% yield. Mp 206.5–208.1 °C. ^{1}H NMR (400 MHz, CD_2Cl_2, ppm): $\delta = 8.97$ (d, $J = 4$ Hz, 2H), 8.92 (d, $J = 4$ Hz, 2H), 7.87 (s, 2H), 7.74 (d, $J = 4$ Hz, 2H), 7.59 (d, $J = 4$ Hz, 2H), 7.35–7.33 (m, 2H), 4.08–4.05 (m, 8H), 1.82–1.79 (m, 4H), 1.43–1.29 (m, 32H), 0.97–0.89 (m, 24H); ^{13}C NMR (100 MHz, $CDCl_3$, ppm): $\delta = 161.7$, 161.5, 153.9, 141.1, 138.9, 135.9, 135.2, 134.2, 132.5, 132.0, 131.1, 129.7, 128.6, 126.9, 116.8, 109.2, 108.1, 93.3, 90.8, 46.1, 46.0, 39.2, 39.1, 30.2, 30.2, 28.4, 23.5, 23.1, 14.1, 14.0, 10.5, 10.5; MS (MALDI-TOF): *m*/*z* calcd for $C_{70}H_{81}N_6O_4S_5$ $(M + H)^+$ 1229.7, found 1229.9; anal. calcd for $C_{70}H_{80}N_6O_4S_5$: C, 68.37; H, 6.56; N, 6.83; S, 13.04; found: C, 68.39; H, 6.55; N, 6.80; S, 12.88%.

Synthesis of DPPTT

Compound **3** (550 mg, 1 mmol), $Pd(PPh_3)_4$ (23.1 mg, 0.02 mmol), and CuI (1.1 mg, 0.006 mmol) were loaded into a flame-dried one-neck flask mounted with a condenser. Degassed/anhydrous toluene (20 mL) and $(i\text{-}Pr)_2NH$ (5 mL) were added, followed by the addition of 2,5-dibromothiazolo[5,4-*d*]thiazole (120 mg, 0.4 mmol). Then, the reaction mixture was heated to 90 °C and stirred overnight. After cooling to room temperature, 25 mL of water was added and the mixture was extracted three times with 25 mL of ethyl acetate. The organic phase was dried over Na_2SO_4 and filtered. Then, the filtrate was concentrated under reduced pressure. The crude product was purified *via* flash chromatography with CH_2Cl_2/*n*-hexane (v/v, 1 : 2) as eluent to afford **DPPTT** (370 mg) in 75% yield. Mp 215.8–217.7 °C. ^{1}H NMR (400 MHz, CD_2Cl_2, ppm): $\delta = 8.87$ (d, $J = 4$ Hz, 2H),

8.78 (d, $J = 4$ Hz, 2H), 7.65 (d, $J = 4$ Hz, 2H), 7.52 (d, $J = 4$ Hz, 2H), 7.24–7.22 (m, 2H), 3.96–3.90 (m, 8H), 1.79–1.77 (m, 4H), 1.27–1.18 (m, 32H), 0.84–0.76 (m, 24H); ^{13}C NMR (100 MHz, $CDCl_3$, ppm): $\delta = 161.7, 161.4, 151.7, 150.0, 141.7, 138.3, 136.2, 135.3, 134.9, 133.3, 131.4, 129.6, 128.6, 124.6, 109.7, 108.0, 90.6, 90.4, 46.1, 46.0, 39.3, 39.1, 30.2, 30.1, 29.7, 29.3, 28.4, 28.3, 27.2, 23.6, 23.1, 14.1, 14.0, 10.5, 10.5$; MS (MALDI-TOF): m/z calcd for $C_{68}H_{79}N_6O_4S_6$ $(M + H)^+$ 1235.8, found 1235.4; anal. calcd for $C_{68}H_{78}N_6O_4S_6$: C, 66.09; H, 6.36; N, 6.80; S, 15.57; found: C, 66.18; H, 6.41; N, 6.72; S, 15.48%.

Synthesis of DPPBZ

Compound **1** (600 mg, 1.0 mmol), $Pd(PPh_3)_4$ (23.1 mg, 0.02 mmol), and CuI (1.1 mg, 0.006 mmol) were loaded into a flame-dried one-neck flask mounted with a condenser. Degassed/anhydrous toluene (20 mL) and $(i\text{-}Pr)_2NH$ (5 mL) were added, followed by the addition of 1,4-diethynylbenzene (50.4 mg, 0.4 mmol). Then, the reaction mixture was heated to 90 °C and stirred overnight. After cooling to room temperature, 25 mL of water was added and the mixture was extracted three times with 25 mL of ethyl acetate. The organic phase was dried over Na_2SO_4 and filtered. Then, the filtrate was concentrated under reduced pressure. The crude product was purified *via* flash chromatography with CH_2Cl_2/*n*-hexane (v/v, 1 : 2) as eluent to afford **DPPBZ** (431 mg) in 92% yield. Mp 215.1–218.4 °C. ^{1}H NMR (400 MHz, CD_2Cl_2, ppm): $\delta = 8.83$ (d, $J = 4$ Hz, 2H), 8.78 (d, $J = 4$ Hz, 2H), 7.62 (d, $J = 4$ Hz, 2H), 7.49 (m, 4H), 7.36 (d, $J = 4$ Hz, 2H), 7.22 (m, 2H), 3.94–3.91 (m, 8H), 1.80–1.78 (m, 4H), 1.30–1.18 (m, 32H), 0.84–0.76 (m, 24H); ^{13}C NMR (100 MHz, CD_2Cl_2, ppm): $\delta = 161.5, 161.4, 154.0, 141.0, 138.6, 135.5, 134.9, 134.0, 132.5, 132.2, 131.2, 129.9, 128.4, 126.7, 116.7, 109.3, 108.1, 93.3, 90.4, 45.8, 45.7, 39.2, 39.1, 30.1, 28.3, 23.5, 23.1, 13.8, 13.8, 10.2$; MS (MALDI-TOF): m/z calcd for $C_{70}H_{83}N_4O_4S_4$ $(M + H)^+$ 1171.7, found 1170.7; anal. calcd for $C_{70}H_{82}N_4O_4S_4$: C, 71.76; H, 7.05; N, 4.78; S, 10.94; found: C, 71.60; H, 7.14; N, 4.56; S, 10.59%.

Fabrication of OFET devices

Bottom contact OFETs were fabricated. A heavily doped n-type Si wafer and a layer of dry oxidized SiO_2 (300 nm, with roughness lower than 0.1 nm and a capacitance of 11 nF cm^{-2}) were used as a gate electrode and gate dielectric layer, respectively. The drain–source (D–S) gold contacts were fabricated by photolithography. The substrates were cleaned using deionized water, alcohol, and rinsed in acetone. Then, the surface was modified with *n*-octadecyltrichlorosilane (OTS). Next, the substrates were cleaned in *n*-hexane and $CHCl_3$. The system was stirred for 60 min and the substrates were washed with EtOH. **DPPBT**, **DPPTT** and **DPPBZ** were dissolved in $CHCl_3$ (about 10 mg mL^{-1}) and spin-coated on the surface of the substrates at 2000 rpm. The annealing process was carried out in vacuum for 1 h at each annealing temperature. Field-effect characteristics of the devices were determined in nitrogen using a Keithley 4200 SCS semiconductor parameter analyzer.

The mobility of the OFETs in the saturation region was calculated using the following equation:

$$I_{DS} = \frac{W}{2L}\mu C_i(V_{GS} - V_{th})^2$$

where I_{DS} is the drain electrode collected current; L and W are the channel length and width, respectively; μ is the mobility of the device; C_i is the capacitance per unit area of the gate dielectric layer; V_{GS} is the gate voltage, and V_{th} is the threshold voltage. The V_{th} of the device was determined by extrapolating the $(I_{DS,sat})^{1/2}$ *vs.* V_{GS} plot to $I_{DS} = 0$.

Fabrication of organic photovoltaic cells

OPVs were fabricated with ITO as the positive electrode and Al as the negative electrode. The patterned tin oxide (ITO) glass (sheet resistance = 15 Ω^{-1}) was pre-cleaned in an ultrasonic bath of acetone and isopropyl alcohol and treated in an ultraviolet-ozone chamber (Jelight Company, USA) for 30 min. A thin layer (30 nm) of poly(3,4-ethylenedioxythiophene):poly(styrene sulfonate) (PEDOT:PSS, Baytron PVP AI 4083, Germany) was spin-coated onto the ITO glass and baked at 150 °C for 15 min. Subsequently, a chloroform solution of **DPPBT** or **DPPTT** with $PC_{71}BM$ was spin-coated on the PEDOT:PSS layer to form the active layer. The thickness (*ca.* 80–100 nm) of the active layer was measured using an Ambios Technology XP-2 profilometer. Then, a Ca (*ca.* 20 nm) and aluminium layer (*ca.* 70 nm) were evaporated onto the surface of the active layer under vacuum (*ca.* 10^{-5} Pa) to form the negative electrode. The active area of the device was 4.0 mm^2. The *J–V* curves were measured with a computer-controlled Keithley 236 Source Measure Unit. A xenon lamp coupled with AM1.5 solar spectrum filters was used as the light source, and the optical power at the sample was 100 mW cm^{-2}. The incident photon to converted current efficiency (IPCE) spectra was measured using a Stanford Research Systems model SR830 DSP lock-in amplifier coupled with a WDG3 monochromator and a 500 W xenon lamp.

Acknowledgements

The present research was financially supported by Chinese Academy of Sciences, NSFC and State Key Basic Research Program. The authors thank Prof. Yongfang Li for helpful discussions and allowance for using the facility for the fabrication of OPVs. The authors also gratefully acknowledge the assistance of the scientists of Diffuse X-ray Scattering Station at Beijing Synchrotron Radiation Facility for measuring the GIXRD data. ESI† is available online.

Notes and references

1 W. K. Man, Y. Chen, Z. Peng and L. P. Yu, *J. Am. Chem. Soc.*, 1993, **115**, 11735.

2 (*a*) S. Qu and H. Tian, *Chem. Commun.*, 2012, **48**, 3039; (*b*) C. B. Nielsen, M. Turbiez and I. McCulloch, *Adv. Mater.*, 2013, **25**, 1859; (*c*) Y. Zhao, Y. L. Guo and Y. Q. Liu, *Adv. Mater.*, 2013, **25**, 5372; (*d*) Z. T. Liu, G. X. Zhang, Z. X. Cai, X. Chen, H. W. Luo, Y. H. Li, J. G. Wang and D. Q. Zhang, *Adv. Mater.*, 2014, **26**, 6965.

3 (*a*) Y. N. Li, P. Sonar, L. Murphy and W. Hong, *Energy Environ. Sci.*, 2013, **6**, 1684; (*b*) M. A. Naik and S. Patil, *J. Polym. Sci., Part A: Polym. Chem.*, 2013, **51**, 4241; (*c*) S. Cho, J. Lee, M. Tong, J. H. Seo and C. Yang, *Adv. Funct. Mater.*, 2011, **21**, 1910; (*d*) H. W. Lin, W. Y. Lee and W. C. Chen, *J. Mater. Chem.*, 2012, **22**, 2120; (*e*) J. D. Yuen, R. Kumar, D. Zakhidov, J. Seifter, B. Lim, A. J. Heeger and F. Wudl, *Adv. Mater.*, 2011, **23**, 3780; (*f*) P. T. Wu, F. S. Kim and S. A. Jenekhe, *Chem. Mater.*, 2011, **23**, 4618.

4 (*a*) Y. Qiao, Y. L. Guo, C. M. Yu, F. J. Zhang, W. Xu, Y. Q. Liu and D. B. Zhu, *J. Am. Chem. Soc.*, 2012, **134**, 4084; (*b*) Y. Z. Lin, Y. F. Li and X. W. Zhan, *Adv. Energy Mater.*, 2013, **3**, 724; (*c*) W. Shin, T. Yasuda, G. Watanabe, Y. S. Yang and C. Adachi, *Chem. Mater.*, 2013, **25**, 2549; (*d*) K. Schmidt, C. J. Tassone, J. R. Niskala, A. T. Yiu, O. P. Lee, T. M. Weiss, C. Wang, J. M. J. Fréchet, P. M. Beaujuge and M. F. Toney, *Adv. Mater.*, 2014, **26**, 300; (*e*) H. T. Bai, P. Cheng, Y. F. Wang, L. C. Ma, Y. F. Li, D. B. Zhu and X. W. Zhan, *J. Mater. Chem. A*, 2014, **2**, 778.

5 (*a*) J. Li, Y. Zhao, H. S. Tan, Y. L. Guo, C. A. Di, G. Yu, Y. Q. Liu, M. Lin, S. H. Lim, Y. H. Zhou, H. B. Su and B. S. Ong, *Sci. Rep.*, 2012, **2**, 754; (*b*) J. Lee, A. R. Han, H. Yu, T. J. Shin, C. Yang and J. H. Oh, *J. Am. Chem. Soc.*, 2013, **135**, 9540; (*c*) W. Li, K. H. Hendriks, A. Furlan, W. S. C. Roelofs, M. M. Wienk and R. A. J. Janssen, *J. Am. Chem. Soc.*, 2013, **135**, 18942; (*d*) S. Subramaniyan, F. S. Kim, G. Ren, H. Li and S. A. Jenekhe, *Macromolecules*, 2012, **45**, 9029; (*e*) P. Sonar, S. P. Singh, Y. Li, M. S. Soh and A. Dodabalapur, *Adv. Mater.*, 2010, **22**, 5409; (*f*) M. Shahid, T. McCarthy-Ward, J. Labram, S. Rossbauer, E. B. Domingo, S. E. Watkins, N. Stingelin, T. D. Anthopoulos and M. Heeney, *Chem. Sci.*, 2012, **3**, 181; (*g*) Y. Li, S. P. Singh and P. Sonar, *Adv. Mater.*, 2010, **22**, 4862.

6 (*a*) V. Coropceanu, J. Cornil, D. A. Filho, Y. Olivier, R. Silbey and J. L. Brédas, *Chem. Rev.*, 2007, **107**, 926; (*b*) B. Walker, C. Kim and T. Q. Nguyen, *Chem. Mater.*, 2011, **23**, 470; (*c*) Y. Lin, Y. Li and X. W. Zhan, *Chem. Soc. Rev.*, 2012, **41**, 4245; (*d*) Y. F. Li, *Acc. Chem. Res.*, 2012, **45**, 723.

7 (*a*) A. A. Virkar, S. Mannsfeld, Z. N. Bao and N. Stingelin, *Adv. Mater.*, 2010, **22**, 3857; (*b*) L. Dou, J. You, Z. Hong, Z. Xu, G. Li, R. A. Street and Y. Yang, *Adv. Mater.*, 2013, **25**, 6642; (*c*) Z. He, H. Wu and Y. Cao, *Adv. Mater.*, 2014, **26**, 1006; (*d*) X. K. Gao and Y. B. Hu, *J. Mater. Chem. C*, 2014, **2**, 3099.

8 (*a*) F. S. Kim, X. Guo, M. D. Watson and S. A. Jenekhe, *Adv. Mater.*, 2010, **22**, 478; (*b*) Y. Sun, S. C. Chien, H. L. Yip, Y. Zhang, K. S. Chen, D. F. Zeigler, F. C. Chen, B. Lin and A. K. Y. Jen, *J. Mater. Chem.*, 2011, **21**, 13247; (*c*) M. S. Chen, J. R. Niskala, D. A. Unruh, C. K. Chu, O. P. Lee and J. M. J. Fréchet, *Chem. Mater.*, 2013, **25**, 4088; (*d*) A. D. Scaccabarozzi and N. Stingelin, *J. Mater. Chem. A*, 2014, **2**, 10818.

9 (*a*) V. Steinmann, N. M. Kronenberg, M. R. Lenze, S. M. Graf, D. Hertel, K. Meerholz, H. Bürckstümmer, E. V. Tulyakova and F. Würthner, *Adv. Energy Mater.*, 2011, **1**, 888; (*b*) H. Bürckstümmer, E. V. Tulyakova, M. Deppisch, M. R. Lenze, N. M. Kronenberg, M. Gsanger, M. Stolte, K. Meerholz and F. Würthner, *Angew. Chem., Int. Ed.*, 2011, **50**, 11628.

10 Y. Sun, G. C. Welch, W. L. Leong, C. J. Takacs, G. C. Bazan and A. J. Heeger, *Nat. Mater.*, 2012, **11**, 44.

11 (*a*) P. L. T. Boudreault, J. W. Hennek, S. Loser, R. P. Ortiz, B. J. Eckstein, A. Facchetti and T. J. Marks, *Chem. Mater.*, 2012, **24**, 2929; (*b*) S. Loser, H. Miyauchi, J. W. Hennek, J. Smith, C. Huang, A. Facchetti and T. J. Marks, *Chem. Commun.*, 2012, **48**, 8511.

12 (*a*) L. Ye, S. Zhang, W. Ma, B. Fan, X. Guo, Y. Huang, H. Ade and J. H. Hou, *Adv. Mater.*, 2012, **24**, 6335; (*b*) X. Zhang, Z. Lu, L. Ye, C. Zhan, J. Hou, S. Zhang, B. Jiang, Y. Zhao, J. Huang, S. Zhang, Y. Liu, Q. Shi, Y. Q. Liu and J. N. Yao, *Adv. Mater.*, 2013, **25**, 5791.

13 (*a*) R. Shivanna, S. Shoaee, S. Dimitrov, S. K. Kandappa, S. Rajaram, J. R. Durrant and K. S. Narayan, *Energy Environ. Sci.*, 2014, **7**, 435; (*b*) X. Li, J. Smith, S. Tierney, R. Sweeney, B. K. C. Kjellander, G. H. Gelinck, T. D. Anthopoulos and N. Stingelin, *J. Mater. Chem.*, 2012, **22**, 9458; (*c*) M. A. Hashimi, M. A. Baklar, F. Colleaux, S. E. Watkins, T. D. Anthopoulos, N. Stingelin and M. Heeney, *Macromolecules*, 2011, **44**, 5194.

14 (*a*) S. Roquet, A. Cravino, P. Leriche, O. Aleque, P. Frevemes and J. Roncali, *J. Am. Chem. Soc.*, 2006, **128**, 3459; (*b*) L. Y. Lin, Y. H. Chen, Z. Y. Huang, H. W. Lin, S. H. Chou, F. Lin, C. W. Chen, Y. H. Liu and K. T. Wong, *J. Am. Chem. Soc.*, 2011, **133**, 15822; (*c*) Y. H. Chen, L. Y. Lin, C. W. Lu, F. Lin, Z. Y. Huang, H. W. Lin, P. H. Wang, Y. H. Liu, K. T. Wong, J. Wen, D. J. Miller and S. B. Darling, *J. Am. Chem. Soc.*, 2012, **134**, 13616.

15 (*a*) J. Huang, C. L. Zhan, X. Zhang, Y. Zhao, Z. Lu, H. Jia, B. Jiang, J. Ye, S. Zhang, A. Tang, Y. Q. Liu, Q. B. Pei and J. N. Yao, *ACS Appl. Mater. Interfaces*, 2013, **5**, 2033; (*b*) H. W. Luo, S. J. Chen, Z. T. Liu, C. Zhang, Z. X. Cai, X. Chen, G. X. Zhang, Y. S. Zhao, S. Decurtins, S. X. Liu and D. Q. Zhang, *Adv. Funct. Mater.*, 2014, **24**, 4250.

16 (*a*) R. Fitzner, E. Osteritz, A. Mishra, G. Schulz, E. Reinold, M. Weil, C. Körner, H. Ziehlke, C. Elschner, K. Leo, M. Riede, M. Pfeiffer, C. Uhrich and P. Bäuerle, *J. Am. Chem. Soc.*, 2012, **134**, 11064; (*b*) M. Weidelener, C. D. Wessendorf, J. Hanisch, E. Ahlswede, G. Gotz, M. Linden, G. Schulz, E. M. Osteritz, A. Mishra and P. Bäuerle, *Chem. Commun.*, 2013, **49**, 10865; (*c*) A. Amacher, C. Y. Yi, J. B. Yang, M. P. Bircher, Y. C. Fu, M. Cascella, M. Grätzel, S. Decurtins and S. X. Liu, *Chem. Commun.*, 2014, **50**, 6540.

17 (*a*) Z. M. Tang, T. Lei, K. J. Jiang, Y. L. Song and J. Pei, *Chem.–Asian J.*, 2010, **5**, 1911; (*b*) C. M. Yu, C. He, Y. Yang, Z. X. Cai, H. W. Luo, W. Q. Li, Q. Peng, G. X. Zhang, Z. T. Liu and D. Q. Zhang, *Chem.–Asian J.*, 2014, **9**, 1570.

18 (*a*) E. Ripaud, T. Rousseau, P. Leriche and J. Roncali, *Adv. Energy Mater.*, 2011, **1**, 540; (*b*) Y. Lin, P. Cheng, Y. Li and X. W. Zhan, *Chem. Commun.*, 2012, **48**, 4773; (*c*) Y. S. Chen, X. J. Wan and G. K. Long, *Acc. Chem. Res.*, 2013, **46**, 2645.

19 (*a*) W. Jiang, L. Ye, X. Li, C. Xiao, F. Tan, W. Zhao, J. Hou and Z. Wang, *Chem. Commun.*, 2013, **50**, 1024; (*b*) M. Löbert,

A. Mishra, C. Uhrich, M. Pfeiffer and P. Bäuerle, *J. Mater. Chem. C*, 2014, **2**, 4879.

20 (*a*) S. Dong, H. Zhang, L. Yang, M. Bai, Y. Yao, H. Chen, L. Gan, T. Yang, H. Jiang, S. Hou, L. Wan and X. F. Guo, *Adv. Mater.*, 2012, **24**, 5576; (*b*) Q. Q. Shi, P. Cheng, Y. F. Li and X. W. Zhan, *Adv. Energy Mater.*, 2012, **2**, 63; (*c*) P. Cheng, Q. Q. Shi, Y. Z. Lin, Y. F. Li and X. W. Zhan, *Org. Electron.*, 2013, **14**, 599; (*d*) Y. Z. Lin, H. J. Fan, Y. F. Li and X. W. Zhan, *Adv. Mater.*, 2012, **24**, 3087.

21 (*a*) B. Walker, A. B. Tamayo, X. D. Dang, P. Zalar, J. H. Seo, A. Garcia, M. Tantiwiwat and T. Q. Nguyen, *Adv. Funct. Mater.*, 2009, **19**, 3063; (*b*) S. Loser, C. J. Bruns, H. Miyauchi, R. P. Ortiz, A. Facchetti, S. I. Stupp and T. J. Marks, *J. Am. Chem. Soc.*, 2011, **133**, 8142; (*c*) Y. Z. Lin, L. C. Ma, Y. F. Li, Y. Q. Liu, D. B. Zhu and X. W. Zhan, *Adv. Energy Mater.*, 2013, **3**, 1166.

22 (*a*) Z. X. Cai, H. W. Luo, P. L. Qi, J. G. Wang, G. X. Zhang, Z. T. Liu and D. Q. Zhang, *Macromolecules*, 2014, **47**, 2899; (*b*) D. Gentili, P. Sonar, F. Liscio, T. Cramer, L. Ferlauto, F. Leonardi, S. Milita, A. Dodabalapur and M. Cavallini, *Nano Lett.*, 2013, **13**, 3643.

23 (*a*) Z. X. Cai, H. W. Luo, X. Chen, G. X. Zhang, Z. T. Liu and D. Q. Zhang, *Chem.–Asian J.*, 2014, **9**, 1068; (*b*) Y. Zhang, C. Kim, J. Lin and T. Q. Nguyen, *Adv. Funct. Mater.*, 2012, **22**, 97; (*c*) T. L. Chen, Y. Zhang, P. Smith, A. Tamayo, Y. Liu and B. Ma, *ACS Appl. Mater. Interfaces*, 2011, **3**, 2275; (*d*) A. Riaño, P. M. Burrezo, M. J. Mancheño, A. Timalsina, J. Smith, A. Facchetti, T. J. Marks, J. T. L. Navarrete, J. L. Sequra, J. Casado and R. P. Ortiz, *J. Mater. Chem. C*, 2014, **2**, 6376; (*e*) Y. Wang, Q. Huang, Z. Liu and H. Li, *RSC Adv.*, 2014, **4**, 29509.

24 (*a*) H. Xu, Y. C. Zhou, X. Y. Zhou, K. Liu, L. Y. Cao, Y. Ai, Z. P. Fan and H. L. Zhang, *Adv. Funct. Mater.*, 2014, **24**, 2907; (*b*) J. Li, X. L. Qiao, Y. Xiong, W. Hong, X. K. Gao and H. X. Li, *J. Mater. Chem. C*, 2013, **1**, 5128.